International Journal of Microwave and Wireless Technologies

cambridge.org/mrf

Compact wideband folded strip monopole antenna for brain stroke detection

Payal Bhardwaj[1] and Ritesh Kumar Badhai[2]

[1]Department of Electronics and Communication Engineering, Birla Institute of Technology, Deoghar Campus, Deoghar, Jharkhand, India and [2]Department of Electronics and Communication Engineering, Birla Institute of Technology, Patna Campus, Patna, Bihar, India

Research Paper

Cite this article: Bhardwaj P, Badhai RK (2021). Compact wideband folded strip monopole antenna for brain stroke detection. *International Journal of Microwave and Wireless Technologies* **13**, 937–946. https://doi.org/10.1017/S1759078720001579

Received: 19 May 2020
Revised: 29 October 2020
Accepted: 2 November 2020
First published online: 27 November 2020

Keywords:
Body area network (BAN); brain stroke detection; brain tissue model; specific absorption rate (SAR); ultra-wideband antenna (UWB)

Author for correspondence:
Ritesh Kumar Badhai,
E-mail: riteshkbadhai@bitmesra.ac.in

Abstract

This paper introduces the CPW fed monopole antenna operating at multiple frequencies covering Ultra High Frequency (UHF) bands, suitable for biomedical applications. The planar antenna structure comprises an open loop and a dual folded monopole of optimized length. The antenna exhibits ultra-wideband frequency of operation ranges from 740 MHz to 4.02 GHz covering the frequency bands suitable for head imaging and heart failure detection. The proposed antenna has a compact size of $0.098\lambda \times 0.079\lambda \times 0.019\lambda$ where λ indicates wavelength corresponding to the lowest operating frequency. The antenna is further simulated on the human head model to corroborate applications for brain stroke detection. The specific absorption rate (SAR) value of the proposed antenna is compliant with SAR requirements set by IEEE standards. To experimentally verify the parameters of the proposed antenna design, the antenna is tested on the brain tissue model prepared by materials having dielectric properties like human brain tissue. The peak gain of the antenna, when tested on the human phantom, is 6.8 dBi.

Introduction

The continuous advancement in technology has led to the development of communication systems that offer numerous services in various applications. IR Wireless transmission, Satellite communications, Bluetooth, Wi-Fi, Zigbee, Radio Broadcast, Home Automation Systems, Sensing Systems are few applications that are in tremendous use and are ruling the world. These services widely utilize wireless networks that offer advantages of being cost-effective, convenient to use as it is exempted from the use of cables, provides flexibility in terms of location of the device and the user. Antennas play an important role in the field of mobile communication as well. The wireless wide area network comprising of Universal Mobile Telecommunications System (UMTS) band covering 1.92-2.17GHz band, Long-Term Evolution (LTE) covering 2.5-2.69GHz, WLAN-based network covering 2.4-2.485GHz band are few rapidly growing fields simplifying the integration of mobile and internet services. The multiband antenna uses a folded strip [1-3], slot-loading [4], and electromagnetic coupling [5], gained notable attention in recent years providing better aspect for covering multiple frequency bands.

The healthcare or medical industry is one of the widely growing fields that have been greatly influenced by the emerging wireless technology with a focus on Body Area Network (BAN)[6–9]. Portable microwave-based techniques employed for brain stroke detection[10–15], microwave-based imaging [16], use of microwave cameras for 3D head imaging [17], microwave imaging system for Breast cancer detection [18–20], Pleural Effusion detection (detection of fluid accumulation within the lungs) for heart and lung failure detection [21–25], tumor detection, biomedical telemetry (allows setting up of transmission link for measurement of physiological signals at a distance) [26–28], Blood Glucose monitoring [29, 30] are a few applications to mention. Antennas are being used in medical implantable devices supporting the application such as retinal implants [31], pacemakers, and cardioverter-defibrillators [32–34] and microstrip antennas have emerged as a promising tool in a number of RF and microwave systems.

A brain stroke is the cause of the highest death in the modern era, just after cardiovascular disease and cancer. The detecting traumatic brain injuries using non-invasive techniques [14, 35, 36] is one of the latest research areas which has seen significant growth in recent years. A hemorrhagic brain stroke has been simulated and validated with the 3D model, using a custom antenna fabricated on the FR-4 substrate with the overall size of $45 \times 25 \times 7$ mm^3 [37]. The substrate of thickness 1.5 mm is utilized. The antenna is simulated for the frequency range between 500 MHz and 2.5 GHz, and the minimum value of the reflection coefficient is obtained as around −23 dB at 2.2 GHz. However, the antenna comprises of folded structure separated by a distance of 7 mm. In [38] a probe-fed 3-D folded cavity-backed

CAMBRIDGE UNIVERSITY PRESS

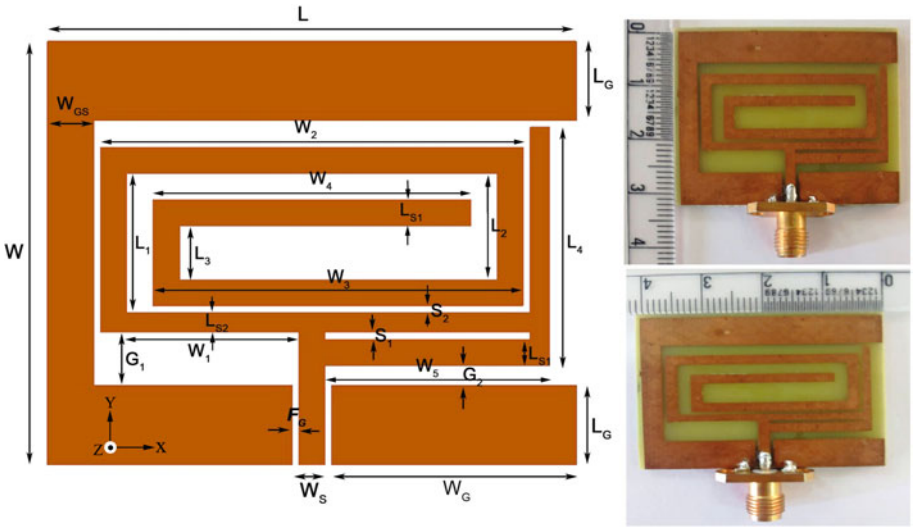

Fig. 1. Proposed antenna structure and prototype.

Table 1. Dimensions of the proposed antenna

Parameters	L	W	L_1	L_2	L_3	L_4	W_1	W_2	W_3	W_4	W_5	L_{S1}
Dimensions (mm)	40	32	10.5	8	4	18	15	32	28	24	17	2
Parameters	L_G	W_G	W_S	W_{GS}	S_1	S_2	G_1	G_2	W_S	F	l_1	l_2
Dimensions (mm)	6	18.5	2	3.5	0.5	0.5	4	1.5	2	0.5	121.5	31

antenna with multi-layer structure for human head diagnosis is proposed with the size of $68 \times 68 \times 22.5$ mm^3, resonating on 1–1.7 GHz band with a small specific absorption rate (SAR) value. This antenna has a large size due to a multi-layer structure. An array of 24 antennas [39] with a final antenna size of 3×4 cm^2 and 1.6 mm thickness, fabricated on a standard FR-4 dielectric substrate, has been designed to obtain a good matching when the antenna is immersed in the coupling medium. The antenna is simulated in the frequency range of 500 MHz to 1.5 GHz and the reflection coefficient below −10 dB is obtained for frequencies from 900 MHz to 1.5 GHz. However, the antenna has not been tested for the SAR, and the effect of radiation not studied when placed close to the human head. A flexible wideband antenna array utilizing electromagnetic bandgap (EBG) and metamaterial unit cells reflector has been proposed [40] with the overall size of $0.29\lambda_0 \times 0.41\lambda_0 \times 0.0198\lambda_0$, where λ_0 corresponds to the wavelength at the center frequency of 1.45 GHz. The array consists of 4×4 radiating patches loaded with symmetrical extended open-ended U-slots and fed by a combination of series and corporate transmission lines operated in contact with the human head. The simulated and measured results show that the antenna has a fractional bandwidth of 53.8% (1.16–1.94 GHz). A trapezoidal-shaped monopole antenna proposed for wearable EM head imaging has been presented [41]. The antenna is designed on FR-4 substrate with 0.2 mm thickness; however, the antenna was not implemented on an EM head imaging system. In recent research, flexible antennas for body area network have gained considerable attention. The extending to brain stroke detection applications, flexible antenna using PET substrate [42, 43] with inkjet printing, polymer technology has been studied.

In the present work, the antenna has been designed for biomedical applications to cover lower frequency bands suitable for microwave imaging and brain stroke detection. Furthermore, the same antenna can be used at higher frequencies for off-body communication. The design comprises of CPW feed, dual folded strip monopole, and open loop structure with optimized length to achieve wide operating bandwidth. Wide operating bandwidth with a fractional bandwidth of 138% is obtained for frequencies from 0.78 to 4.02 GHz, frequencies well suited for brain stroke detection. The structure has been modified in steps by adding monopoles, varying the lengths of the arms of monopoles, introducing slots in the design, and varying loop length.

To evaluate SAR which finds out the amount of power absorbed by human tissue, the human phantom (Head Model) has been introduced using ANSYS simulator and SAR has been calculated to corroborate its applicability for wearable devices as well as for specified brain stroke detection. The values of SAR were found to lie within the standards regulated by IEEE [44]. As per the radiation norms defined by the International Electrotechnical Commission (IEC), the SAR limit on the head is 2 W/kg at average 10 g tissues. However, the FCC and International Commission on Non-Ionizing Radiation Protection (ICNIRP) limits the SAR to 1.6 W/kg per 1g mass tissue, accordingly [45]. To experimentally validate the characteristics of an antenna for a specific application of brain stroke detection, a brain tissue-mimicking model is prepared by using materials with similar electrical properties as head tissue. The experimental results obtained for the model are in good agreement with the simulated results.

Proposed antenna configuration

Antenna design

The proposed folded strip monopole antenna, as shown in Fig. 1, is designed with compact size of $40 \times 32 \times 0.8$ mm^3. The folded

https://doi.org/10.1017/S1759078720001579 Published online by Cambridge University Press

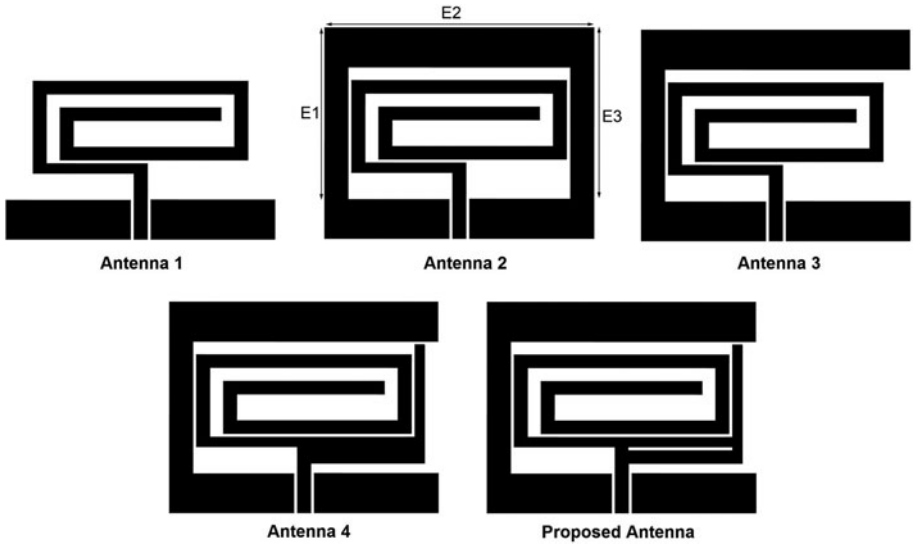

Fig. 2. Progressive developments of the proposed antenna.

strips of copper are printed on FR-4 epoxy substrate with permittivity, $\varepsilon_r = 4.4$ and loss tangent, $(tan\delta) = 0.02$. The design consists of a dual folded strip resonators with optimized length to get broad bandwidth and multiple resonances. The two folded strip radiators are attached to the feed line in opposite directions. The length of folded strip loop $l_1 = (W_1 + L_1 + W_2 + L_2 + W_3 + L_3 + W_4)$ is optimized to a quarter wavelength at the lowest resonating frequency to get multiple resonances i.e. $l_1 = \lambda/4$ at 740 MHz. The length of the second folded strip ($l_2 = W_5 + L_4$) is optimized to $l_2 = \lambda/8$ for achieving the resonance at higher frequencies. The loading of slot (S_1) in the l_2 radiator improves the bandwidth of the response and shifts the resonance to a desired lower frequency band, suitable for bio-medical applications. The proposed antenna dimensions are presented in Table 1.

Resonance analysis

The most suitable frequency reported in the literature for microwave head imaging/brain stroke detection is 1 GHz [46]. This frequency offers a reasonable compromise between the spatial resolution of brain images and the penetration of microwave signals into the human head. Therefore, the frequency-dispersive model is evaluated near the 1 GHz. The resonating frequency of the antenna can be calculated as [47].

$$f_r = \frac{c}{2L_{eff}\sqrt{\varepsilon_{eff}}} \tag{1}$$

Where c is the velocity of light in free space.

$$\varepsilon_{eff} = \frac{\varepsilon_r + 1}{2} + \frac{\varepsilon_r - 1}{2}\left(1 + \frac{12h}{w}\right)^{-1/2} \tag{2}$$

$$\frac{\Delta L}{h} = 0.412\frac{(\varepsilon_{eff} + 0.3)(w/h + 0.264)}{(\varepsilon_{eff} - 0.258)(w/h + 0.8)} \tag{3}$$

$$L_{eff} = L + 2\Delta L \tag{4}$$

With the length of the patch as L and the width as W, relative permittivity (ε_r) and thickness of substrate h.

Antenna configurations

In this section, the design of the proposed antenna is discussed. The progressive evolution of the proposed antenna is shown in Fig. 2. The reflection coefficient ($|S_{11}|$) at a lower frequency band suitable for brain stroke detection is shown in Fig. 3(a). While Fig. 3(b) presents $|S_{11}|$ for upper-frequency bands suitable off-body communication. The design starts with a folded resonating strip and the conventional rectangular ground plane (Antenna 1). Folding the radiating strip increases the electrical path of current on the radiating patch. The folded strip antenna presents multiple resonances, but the reflection coefficient ($|S_{11}|$) is narrowband and not resonating at the desired frequency band of brain stroke detection as shown in Fig. 3. To improve the performance of the antenna, parasitic strips of length 92 mm (E1 +E2+E3) is added to the ground plane (Antenna 2). Proximity coupling between the arms of the folded radiating patch l_1 and parasitic strip results in the generation of resonance at the upper-frequency band and improves the impedance matching at higher frequency bands. It provides wideband between 5.5 and 6.5 GHz, covering UNII bands for WLAN, Wi-Fi, WiMAX, and X-band applications. To achieve resonance at lower frequencies suitable for head imaging/brain stroke detection, a modification in design is required. From simulations, it is noted that, in Antenna 2, most of the coupling exists between the upper arm of the radiator and extended ground strip E2. Therefore, the dimension of the extended ground plane is reduced empirically using a simulation tool to obtain an optimum length of 76 mm (E1+E2) (Antenna 3). The inverted L-shaped open circuit stub acts as a capacitor-fed monopole excited at the low-frequency band. The inverted L-shaped open circuit stub excites lower frequencies, however resonant peaks at upper bands are disturbed. The shift in the return loss values at higher frequencies may be attributed because of open-ended ground length. The antenna design is further improved by introducing a second monopole folded strip to the right of the CPW feed (Antenna 4). The length of monopole strip l_2 is chosen to be $\lambda/8$ at the lowest operating frequency to excite the resonance at higher frequencies. Adding of the optimized folded arm of length 31 mm (Antenna 4) allows redistribution of current. The coupling between the monopole and folded radiator helps achieve resonance at higher frequencies. The

https://doi.org/10.1017/S1759078720001579 Published online by Cambridge University Press

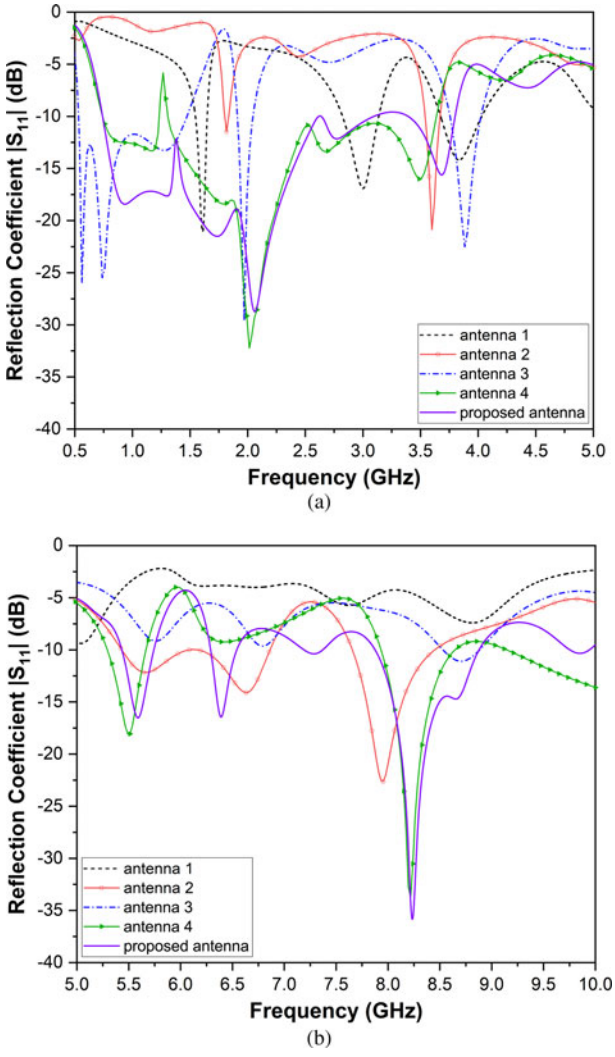

Fig. 3. Comparison of $|S_{11}|$ for initial antenna designs with the proposed monopole antenna (a) 0.5–5 GHz, (b) 5–10 GHz.

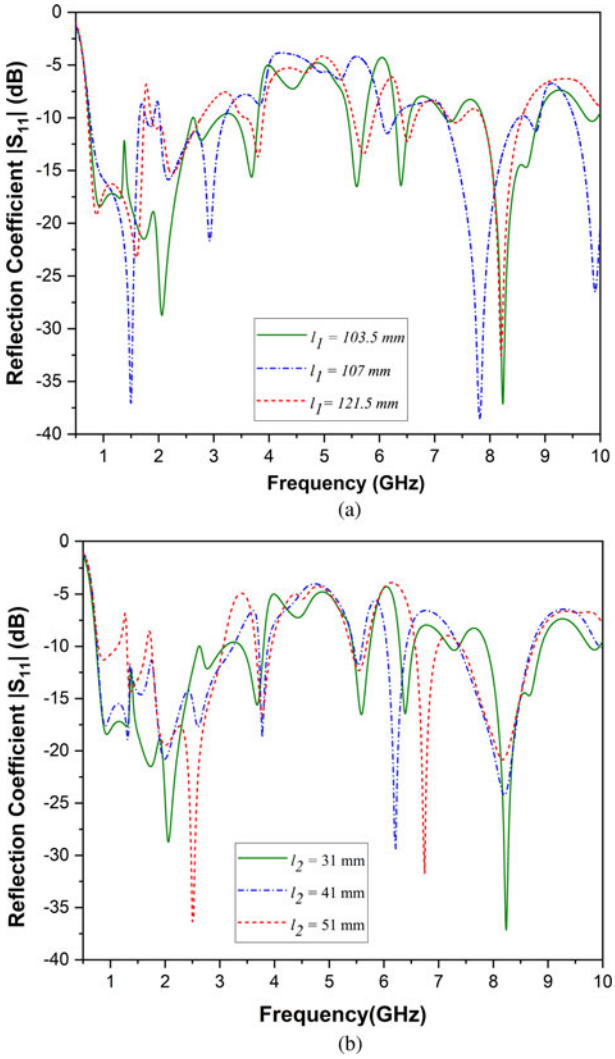

Fig. 4. Effect of folded length on reflection coefficient ($|S_{11}|$) (a) l_1, (b) l_2.

addition of an l_2 resonator improves the impedance matching at higher frequency bands while impedance matching at lower frequency bands is degraded because of the poor coupling between the l_1 and l_2 radiators. The poor coupling diminishes the current distribution at lower frequencies. The antenna design is further improved in the final step, toward the design of the proposed antenna, a slot is introduced in the arm of the second monopole. The slot increases the current path length and contributes to getting lower resonating frequencies. The slotted arm and the ground loop improve the performance of the antenna. The proposed antenna gains the needed impedance matching at lower and higher bands suitable for on-body and off-body applications.

Effect of variation of folded strip length (l_1)

The lowest resonating frequency f_1 of the proposed antenna can be calculated using the empirical formula presented in equation (5),

$$f_1 = \frac{c}{\lambda/4} = \frac{4c}{W_1 + L_1 + W_2 + L_2 + W_3 + L_3 + W_4} \quad (5)$$

where c is the velocity of light in free space. The folded strip length l_1 of the monopole antenna is varied to get the desired frequency band. The effect of the various folded strip length on the reflection coefficient $|S_{11}|$ of the antenna is shown in Fig. 4(a). From the figure, it is seen that for the folded strip length l_1 = 103.5 mm, dual resonance bands are obtained. The impedance matching for the lower and higher frequency bands is good but the impedance matching between 2.0 and 6.4 GHz band is poor. Next, for the l_1=107 mm, multiple resonances are obtained at 1.6, 2.25, 3.8, 5.7, 6.5, and 8.2 GHz. However, it shows a poor impedance matching values at 3.8, 5.7, and 6.5 GHz. Further by increasing the folded arm length l_1 to 121.5 mm, resonance with significant impedance matching ($|S_{11}| \leq -10$ dB) gained. Also, the suitable lower band is covered with a wider bandwidth.

Effect of variation of folded strip length (l_2)

The folded strip length l_2 has its impact on a higher frequency, while the lower frequencies are not much affected by the variation in the l_2 as shown in Fig. 4(b). By increasing the folded strip length l_2, the higher-order bands shifted toward lower resonating

https://doi.org/10.1017/S1759078720001579 Published online by Cambridge University Press

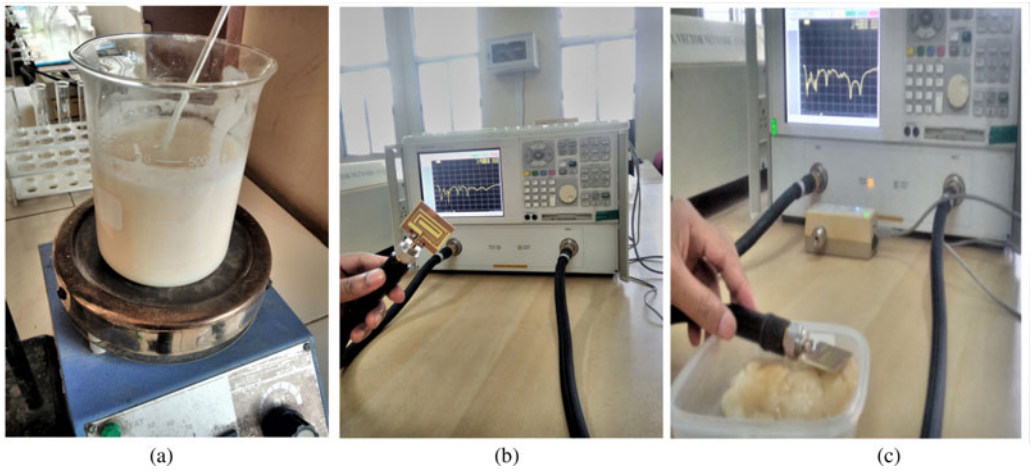

Fig. 5. Experimental set up to demonstrate (a) tissue-mimicking mixture preparation, (b) reflection coefficient free space, and (c) reflection coefficient measurement in the presence of brain tissue-mimicking compound.

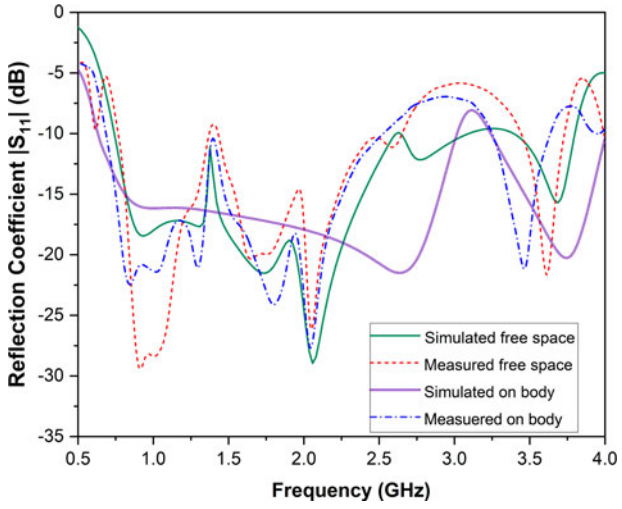

Fig. 6. Simulated and measured reflection coefficient ($|S_{11}|$) of the proposed antenna in free space and human head phantom.

frequencies because of the increase in the electrical length of the radiator. The effect of folded strip l_2 on the reflection coefficient of the antenna is considered for the length of l_2 = 31, 41, and 51 mm, while the l_1 is kept constant at 121.5 mm. The better impedance matching for WiMAX, WLAN, and X-band application is gained at l_2 = 31 mm.

Results and discussion

The proposed antenna design simulated on a high-frequency EM simulator (HFSS). The antenna simulated in free space and in the proximity of the human head phantom. The proposed antenna prototype is fabricated on a glass epoxy FR-4 substrate. The designed antenna is further tested in free space and on brain mimicking tissue. The low-cost brain-mimicking tissue represents the soft tissues of the human brain. The different percentages of Propylene Glycol, Sodium Azide, Corn Flour, Gelatin, and distilled water are taken to prepare low-cost brain tissue sample [48]. The mixture is heated at desired temperatures with constant stirring using the magnetic stirrer to form a semi-solid compound. The experimental setup to prepare tissue mimic mixture and the reflection coefficient measurement in free space and in the vicinity of the brain tissue model is shown in Fig. 5.

Reflection coefficient

The reflection coefficient ($|S_{11}|$) measurement of the proposed antenna is performed using AGILENT PNA-LN5230A Vector Network Analyzer. The antenna, when tested on Human head phantom, showed significant values of reflection coefficient with

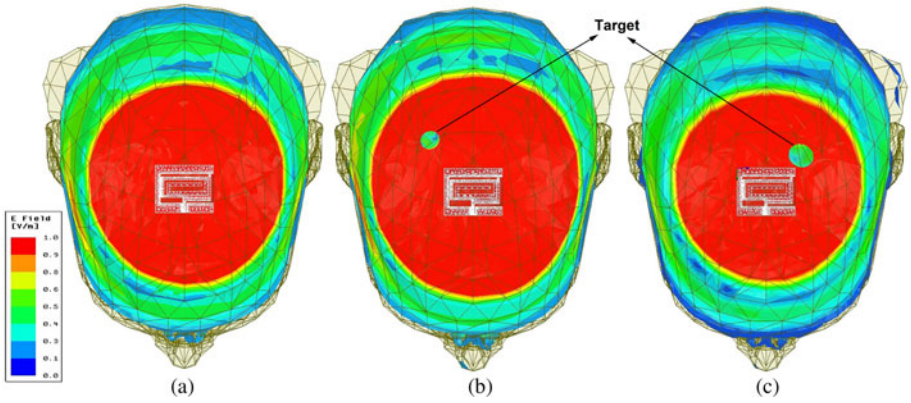

Fig. 7. The normalized electric field distribution on human head phantom at 1 GHz (a) normal brain, (b) hemorrhage target r = 7 mm, and (c) hemorrhage target r = 10 mm.

https://doi.org/10.1017/S1759078720001579 Published online by Cambridge University Press

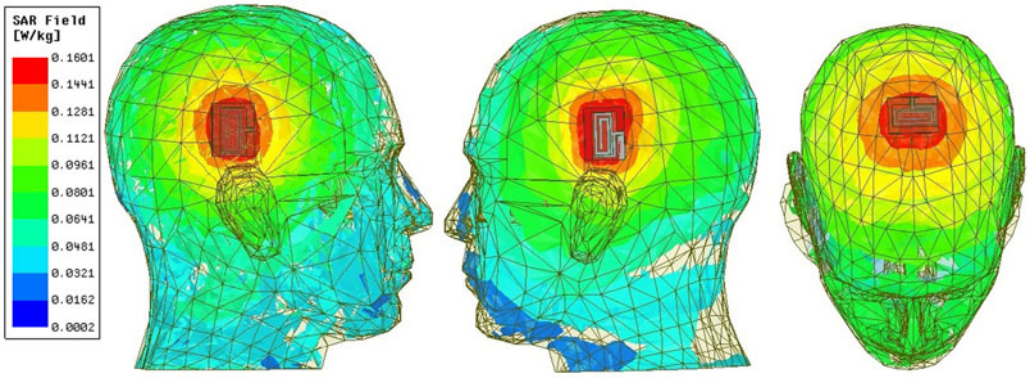

Fig. 8. SAR determination on human head model for input power of 10 dBm at a distance of 5 mm resonating at 1 GHz.

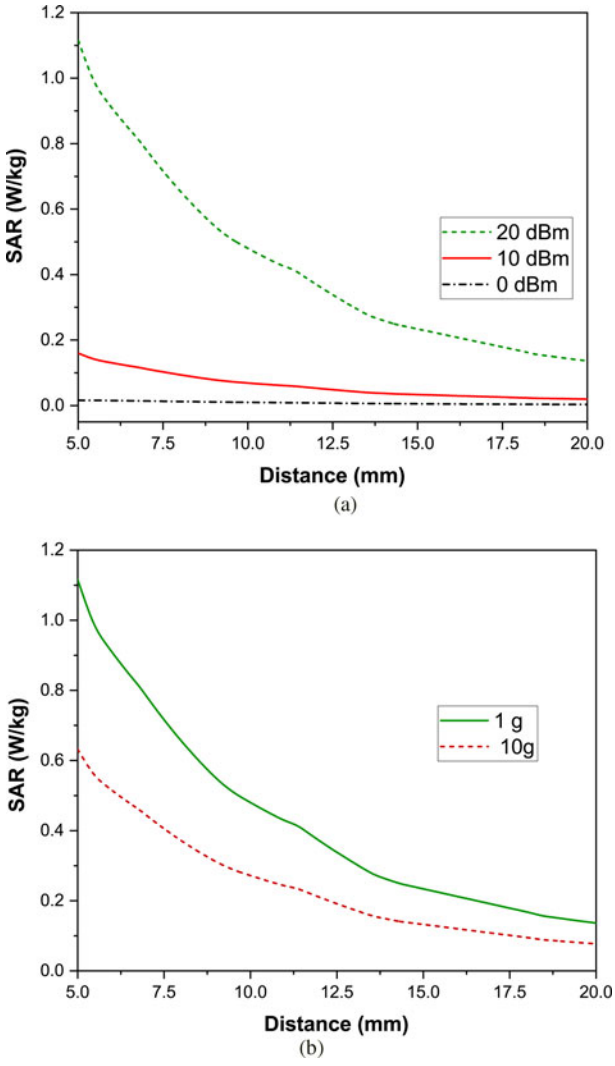

Fig. 9. Variation of average SAR due to the separation distance between the human head phantom and the proposed antenna at 1 GHz for (a) different input powers, (b) 1 gm and 10 g tissue mass for 20 dBm input power.

good impedance matching at desired frequencies. The plot of $|S_{11}|$ shows a wide operating bandwidth at frequencies desirable for brain stroke detection. The ultra-wideband (UWB) operation is achieved for frequencies 0.78–4.02 GHz, frequencies well suited for brain stroke detection. The proposed antenna can also resonate at 2.4, 3.6, 5.6, 8.2 GHz for ISM band (2.40–2.48 GHz), WiMAX (3.3–3.6 GHz), WLAN UNII-2 (5.40–5.75 GHz) and also the 8 GHz band can be utilized for satellite X-band applications. The simulated and measured reflection coefficients of the proposed antenna in free space as well as on the human head phantom are shown in Fig. 6.

Table 2. Simulated average specific absorption rate (SAR) at the center frequency of 1 GHz

Incident power (mW)	Average SAR (1 g) (W/Kg)
1	0.016
10	0.16
100	1.16
125	1.54
150	1.85
200	2.46

Electric field distribution

The proposed antenna is placed at the top of the human head phantom at the separation of 5 mm from the surface of the head phantom. The electric field distribution on the human head is simulated at 1 GHz. The spherical shape hemorrhage target (permittivity (ε_r) = 61.065 and conductivity (σ) = 1.5829 S/m) with a radius of 7 and 10 mm are located in the brain at a depth of 50 mm from the top surface of the head. The electric field distribution of the proposed antenna for a healthy brain and brain with hemorrhage stroke is shown in Fig. 7. No significant scatterer is observed for a healthy brain. While the lower electric field distribution is observed across the hemorrhage target results from an increase in the absorption, which is presented due to the high conductivity of the target. By analysis of the E-field of normal brain and brain with hemorrhage stroke using digital image processing algorithms, the signature can be visualized as a 2D image.

Specific absorption rate

The adaptability of an antenna for biomedical applications can be evaluated by measuring its SAR. The purpose of the SAR analysis is to describe the energy absorbed by the human head when it is

https://doi.org/10.1017/S1759078720001579 Published online by Cambridge University Press

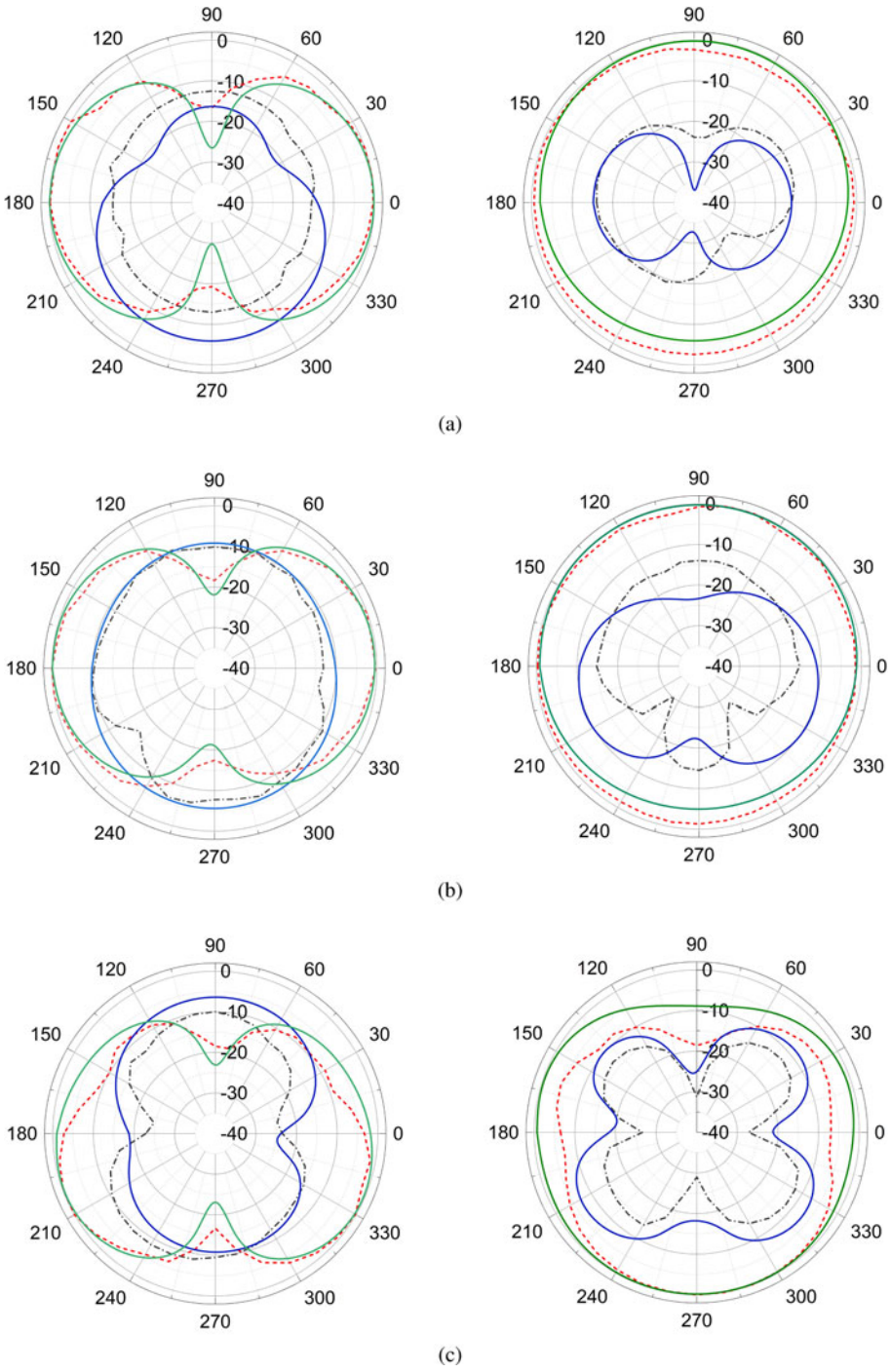

Fig. 10. The simulated and measured normalized radiation pattern of the proposed antenna E-plane (Left side) and H-plane (right side) at (a) 1 GHz, (b) 2.05 GHz, (c) 5.60 GHz, and (d) 8.24 GHz.

exposed in RF electromagnetic field produced by the proposed antenna and its value should comply with the Institute of Electrical and Electronics Engineers (IEEE C95.1 standard), which restricts SAR values averaged over 1 g of any tissue to be less than 1.6 W/kg. For on-body applications where tissue serves as a propagation channel, tissue conductivity, and frequency-dependent electric fields are factors that affect the precise determination of SAR. The SAR is related to the electric field and temperature at a point by the equation (6) [49].

$$SAR = \frac{\sigma|\mathbf{E}|^2}{\rho} - c\frac{\Delta T}{\Delta t} \tag{6}$$

where ρ is the mass density of the tissue (kg/m^3), E is the RMS electric field strength (V/m), ΔT is the change in temperature (K), Δt is the duration of exposure in seconds, and c is the specific heat capacity (J/kg). Low SAR indicates low near field radiations as SAR is proportional to the square of the magnitude of the electric field. The maximum average SAR for the proposed antenna is obtained to be 0.016, 0.16, and 1.16 W/kg for the input power of 0, 10, and 20 dBm respectively averaged over 1 g of tissue, when placed at a distance of 5 mm from the head model. The values lie within range so as not to cause any undesirable impact when placed near the head. The SAR for the proposed antenna for three positions of the brain is shown in Fig. 8. The effect of the distance between the human head phantom and the antenna on

https://doi.org/10.1017/S1759078720001579 Published online by Cambridge University Press

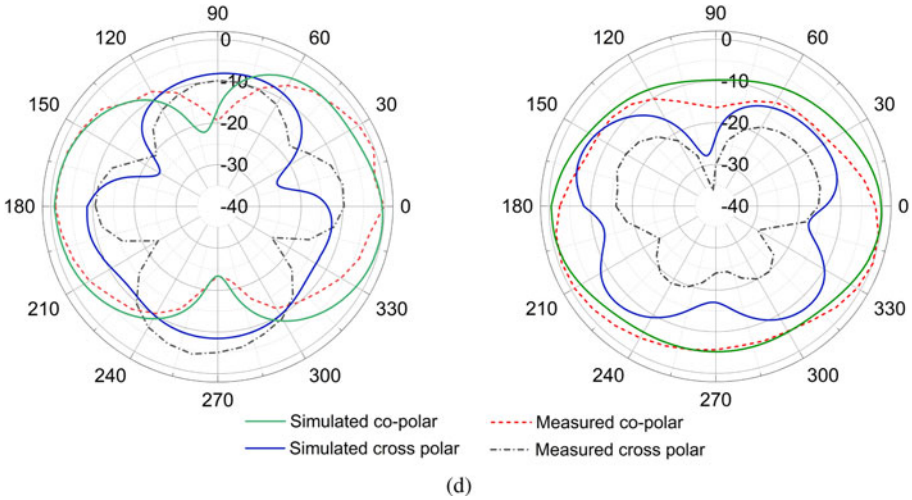

Fig. 10. Continued.

Table 3. Comparison of proposed antenna design with similar literature

Reference	Operating frequency band (GHz)	Bandwidth (%)	Size (mm^3)	Gain (dB)	SAR (W/Kg)
[11]	1.25–2.40	63	70 × 30.5 × 15	3.5	0.17
[12]	1.23–2.56	70.1	70 × 15 × 7	3.82	*
[13]	1.25–2.4	63	70 × 45 × 15	3.5	*
[14]	1.1–2.45	76	81.2 × 80 × 1.6	4.5	*
[36]	1.1–3.4	102.2	70 × 30 × 15	4.0	*
[38]	1.0–1.7	51.8	68 × 68 × 22.5	*	0.0147
[40]	1.16–1.94	50.3	85 × 60 × 2.5	3.5	0.5
[41]	1.3–3.5	91.7	70 × 30 × 0.075	5.0	1.7
Proposed	0.74–4.02	137.8	40 × 32 × 0.8	6.8	0.16

*Not reported.

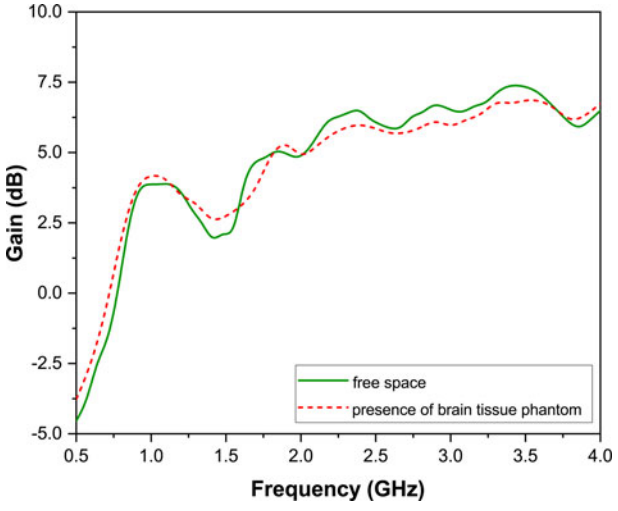

Fig. 11. The measured gain of the antenna in free space and the presence of the human brain tissue phantom.

SAR value for the three different input levels of 0, 10, 20 dBm is plotted in Fig. 9(a). The antenna is also simulated for the average SAR values for 1 and 10 g of tissues mass for an input power of 100 mW (20 dBm) and the calculated values for 1 and 10 g of tissues are 1.16 and 0.63 W/kg respectively, which follow the standard limits defined by ICNIRP and IEEE. The variation in average SAR due to the separation distance between the human head phantom and the proposed antenna for an input power of 20 dBm is shown in Fig. 9(b). It is seen from Fig. 9 that the increase in distance between the human head phantom and the antenna, the average SAR values decrease and vice versa. The SAR analysis also reveals the maximum allowable power. The proposed antenna can be operated up to 125 mW of antenna input power without effecting the human head tissues as shown in Table 2.

Radiation pattern

To ensure that the antenna radiates most of its accepted power in the desired direction, its far-field radiation patterns were simulated and measured at 1, 2.05, 5.6, and 8.24 GHz. The simulated and measured normalized radiation patterns are presented in Fig. 10. The proposed antenna shows monopole-like radiation pattern with the maximum gain in the boresight direction. The antenna radiates in broadside direction in the XZ plane, while an omnidirectional pattern is obtained in the XY plane at 1 and 2.05 GHz. The antenna produces directive radiation patterns for both the plane at 5.6 and 8.24 GHz, which are useful for

https://doi.org/10.1017/S1759078720001579 Published online by Cambridge University Press

communication from on-body to off-body devices. The cross-polarization level is found to be 12 dB lower than co-polarization, both XZ and XY plane at all the operating frequency bands in boresight direction. The measured radiation pattern of the proposed antenna reasonably validates the simulated radiation patterns.

The proposed antenna has a peak gain of 7.1 dB at 3.60 GHz in free space and 6.8 dB at 3.45 GHz in the presence of a human brain tissue phantom. The measured gain plot of the antenna in free space and the human brain tissue phantom is shown in Fig. 11. The characteristics of the proposed antenna are compared with some similar types of papers as presented in Table 3 and found it is suitable for the brain stroke detection application.

Conclusion

This paper illustrates the design of the folded strip monopole antenna for brain stroke detection/imaging applications. The design of the UWB antenna operating at the multiband frequency, makes it suitable for on-body and off-body communication such as WLAN, WiMAX, and X-band communications. The proposed antenna has a compact size, good impedance matching, wideband characteristics, and good radiation pattern with lower SAR values suitable for wearable devices and brain imaging applications. The antenna operates with suitable efficiency and gains over the desired frequency band. The measured results are in close agreement with the simulated results.

References

1. **Beigi P, Zehforoosh Y, Rezvani M and Nourinia J** (2019) Evaluation of a compact triangular crinkle-shaped multiband antenna with circular polarized for ITU band based on MADM method. *Circuit world* **45**, 292–299.
2. **Ashyap AY, Abidin ZZ, Dahlan SH, Majid HA, Waddah AMA, Kamarudin MR, Oguntala GA, Abd-Alhameed RA and Noras JM** (2018) Inverted E-shaped wearable textile antenna for medical applications. *IEEE Access* **6**, 35214–35222.
3. **Beigi P, Nourinia J and Zehforoosh Y** (2018) Compact CPW-fed spiral-patch monopole antenna with tuneable frequency for multiband applications. *Journal of Instrumentation* **13**, P04014.
4. **Li X, Sit YL, Zwirello L and Zwick T** (2013) A miniaturized UWB stepped-slot antenna for medical diagnostic imaging. *Microwave and Optical Technology Letters* **55**, 105–109.
5. **Fatolahzadeh N and Zehforoosh Y** (2017) Electromagnetically coupled elliptical antenna for UWB and WLAN/WiMAX systems. *Microwave and Optical Technology Letters* **59**, 1321–1326.
6. **Jiang ZH, Cui Z, Yue T, Zhu Y and Werner DH** (2017) Compact highly efficient, and fully flexible circularly polarized antenna enabled by silver nanowires for wireless body-area networks. *IEEE Transactions on Biomedical Circuits and Systems* **11**, 920–932.
7. **Ashyap AYI, Zainal Abidin Z, Dahlan SH, Majid HA, Shah SM, Kamarudin MR and Alomainy A** (2017) Compact and low-profile textile ebg-based antenna for wearable medical applications. *IEEE Antennas and Wireless Propagation Letters* **16**, 2550–2550.
8. **Abbasi MAB, Nikolaou SS, Antoniades MA, Nikolić Stevanović M and Vryonides P** (2017) Compact ebg-backed planar monopole for ban wearable applications. *IEEE Transactions on Antennas and Propagation* **65**, 453–463.
9. **Kumar A, Badhai RK and Suraj P** (2018) Design of a printed symmetrical cpw-fed monopole antenna for on-body medical diagnosis applications. *Journal of Computational Electronics* **17**, 1741–1747.
10. **Mohammed BJ, Ireland D and Bialkowsk ME** (2012) Compact wideband antenna for microwave imaging of brain. *Progress In Electromagnetics Research C* **27**, 27–39.
11. **Mobashsher AT and Abbosh A** (2014) Development of compact directional antenna utilising plane of symmetry for wideband brain stroke detection systems. *Electronics Letters* **50**, 850–851.
12. **Das TK and Behera SK** (2017) Design of a 3D cross-fed antenna for microwave-based head imaging applications. *in IEEE Applied Electromagnetics Conference (AEMC)*, pp. 1–2.
13. **Mobashsher AT and Abbosh AM** (2016) Performance of directional and omnidirectional antennas in wideband head imaging. *IEEE Antennas and Wireless Propagation Letters* **15**, 1618–1621.
14. **Wu Y and Pan D** (2018) Directional folded antenna for brain stroke detection based on classification algorithm. *IEEE 4th Information Technology and Mechatronics Engineering Conference (ITOEC), IEEE*, pp. 499–503.
15. **Abtahi S, Yang J and Kidborg S** (2012) A new compact multiband antenna for stroke diagnosis system over 0.5–3 GHz. *Microwave and Optical Technology Letters* **54**, 2342–2346.
16. **Abbak M, Özgür S and Akduman I** (2015) Shorted stacked antenna with folded feed for microwave detection of brain stroke. *in 23rd Telecommunications Forum Telfor (TELFOR), IEEE*, pp. 603–606.
17. **Ghasr MT, Horst MJ, Dvorsky MR and Zoughi R** (2017) Wideband microwave camera for real-time 3-d imaging. *IEEE Transactions on Antennas and Propagation* **65**, 258–268.
18. **Bahramiabarghouei H, Porter E, Santorelli A, Gosselin B, Popović M and Rusch LA** (2015) Flexible 16 antenna array for microwave breast cancer detection. *IEEE Transactions on Biomedical Engineering* **62**, 2516–2525.
19. **Shannon CJ, Fear EC and Okoniewski M** (2005) Dielectric-filled slotline bowtie antenna for breast cancer detection. *Electronics Letters* **41**, 388–390.
20. **Aguilar SM, Al-Joumayly MA, Burfeindt MJ, Behdad N and Hagness SC** (2014) Multiband miniaturized patch antennas for a compact, shielded microwave breast imaging array. *IEEE Transactions on Antennas and Propagation* **62**, 1221–1231.
21. **Ahdi Rezaeieh S, Abbosh AM, Zamani A and Bialkowski K** (2015) Pleural effusion detection system using wideband slot-loaded loop antenna. *Electronics Letters* **51**, 1144–1146.
22. **Ahdi Rezaeieh S, Bialkowski KS, Zamani A and Abbosh AM** (2016) Loop-dipole composite antenna for wideband microwave-based medical diagnostic systems with verification on pulmonary edema detection. *IEEE Antennas and Wireless Propagation Letters* **15**, 838–841.
23. **Rezaeiehr S, Zamani A, Bialkowski KS, Mahmoudi A and Abbosh AM** (2015) Feasibility of using wideband microwave system for non-invasive detection and monitoring of pulmonary oedema. *Scientific Reports* **5**, 14047, 1–11.
24. **Ahdi Rezaeieh S, Zamani A, Bialkowski KS and Abbosh AM** (2015) Unidirectional slot-loaded loop antenna with wideband performance and compact size for congestive heart failure detection. *IEEE Transactions on Antennas and Propagation* **63**, 4557–4562.
25. **Kumar A and Badhai RK** (2017) A novel compact printed wideband on-body monopole antenna for the diagnosis of heart failure detection. *International Journal of Control Theory and Applications* **10**, 207–217.
26. **Xiao S, Liu C, Li Y, Yang XM and Liu X** (2016)Small-size dual-antenna implantable system for biotelemetry devices. *IEEE Antennas and Wireless Propagation Letters* **15**, 1723–1726.
27. **Candefjord S, Winges J, Malik AA, Yu Y, Rylander T, McKelvey T, Fhager A, Elam M and Perrson M** (2017) Microwave technology for detecting traumatic intracranial bleedings: tests on phantom of subdural hematoma and numerical simulations. *Medical and Biological Engineering and Computing* **55**, 1177–1188.
28. **Mobashsher AH and Abbosh AM** (2016) On-site rapid diagnosis of intracranial hematoma using portable multi-slice microwave imaging system. *Scientific Reports* **6**, 37620.
29. **Tamborlane WV, Beck RW, Bode BW, Buckingham B, Chase HP, Clemons R, Fiallo-Scharer R, Fox LA, Gilliam LK, Hirsch IB, Huang ES, Kollman C, Kowalski AJ, Laffel L, Lawrence JM, Lee J, Mauras N, O'Grady M, Ruedy KJ, Tansey M, Tsalikian E, Weinzimer S, Wilson DM, Wolpert H, Wysocki T and Xing D** (2008) Continuous glucose monitoring and intensive treatment of type 1 diabetes. *The New England Journal of Medicine* **359**, 1464–1476.

https://doi.org/10.1017/S1759078720001579 Published online by Cambridge University Press

30. **Liu XY, Wu ZT, Fan Y and Tentzeris EM** (2017) A miniaturized csrr loaded wide-beamwidth circularly polarized implantable antenna for subcutaneous real-time glucose monitoring. *IEEE Antennas and Wireless Propagation Letters* **16**, 577–580.
31. **Gosalia K, Lazzi G and Humayun M** (2004) Investigation of a microwave data telemetry link for a retinal prosthesis. *IEEE Transactions on Microwave Theory and Techniques* **52**, 1925–1933.
32. **Shimonov N, Vulfin V, Sayfan-Altman S and Ianconescu R** (2016) Design of an implanted antenna inside the human body for a pacemaker application. *in IEEE International Conference on the Science of Electrical Engineering (ICSEE)*, pp. 1–3.
33. **Yang Z, Zhu L and Xiao S** (2018) An implantable circularly polarized patch antenna design for pacemaker monitoring based on quality factor analysis. *IEEE Transactions on Antennas and Propagation* **66**, 5180–5192.
34. **Wessels D** (2002) Implantable pacemakers and defibrillators: device overview emi considerations. *in IEEE International Symposium on Electromagnetic Compatibility*, Vol. 2.
35. **Mobashsher AT, Bialkowski KS, Abbosh AM and Crozier S** (2016) Design and experimental evaluation of a non-invasive microwave head imaging system for intracranial haemorrhage detection. *PLoS ONE* **11**, 1–29.
36. **Mobashsher AT, Abbosh AM and Wang Y** (2014) Microwave system to detect traumatic brain injuries using compact unidirectional antenna and wideband transceiver with verification on realistic head phantom. *IEEE Transactions on Microwave Theory and Techniques* **62**, 1826–1836.
37. **Bisio I, Estatico C, Fedeli A, Lavagetto F, Pastorino M, Randazzo A and Sciarrone A** (2018) Brain stroke microwave imaging by means of a newton-conjugate-gradient method in L^p banach spaces. *IEEE Transactions on Microwave Theory and Techniques* **66**, 3668–3682.
38. **Rokunuzzaman M, Ahmed A, Baum TC and Rowe WS** (2019) Compact 3-D antenna for medical diagnosis of the human head. *IEEE Transactions on Antennas and Propagation* **67**, 5093–5103.
39. **Scapaticci R, Tobon J, Bellizzi G, Vipiana F and Crocco L** (2018) Design and numerical characterization of a low-complexity microwave device for brain stroke monitoring.*IEEE Transactions on Antennas and Propagation* **66**, 7328–7338.
40. **Alqadami ASM, Bialkowski KS, Mobashsher AT and Abbosh AM** (2019) Wearable electromagnetic head imaging system using flexible wideband antenna array based on polymer technology for brain stroke diagnosis. *IEEE Transactions on Biomedical Circuits and Systems* **13**, 124–134.
41. **Bashri MSR, Arslan T and Zhou W** (2017) Flexible antenna array for wearable head imaging system. *in IEEE 2017 11th European Conference on Antennas and Propagation (EUCAP)*, pp. 172–176.
42. **Rahman MA, Hossain MF, Riheen MA and Sekhar PK** (2020) Early Brain Stroke Detection Using Flexible Monopole Antenna. *Progress In Electromagnetics Research* **99**, 99–110.
43. **Guo X, Hang Y, Xie Z, Wu C, Gao L and Liu C** (2017) Flexible and wearable 2.45 GHz CPW-fed antenna using inkjet-printing of silver nanoparticles on pet substrate. *Microwave and Optical Technology Letters* **59**, 204–208.
44. IEEE Standard for Safety Levels with Respect to Human Exposure to Radio Frequency Electromagnetic Fields, 3 kHz to 300 GHz. *IEEE Std C95.1-2005 (Revision of IEEE Std C95.1-1991)*, 2006, pp. 1–238.
45. **Yahya R, Kamarudin MR and Seman N** (2014) New wideband textile antenna for sar investigation in head microwave imaging. *in IEEE MTT-S International Microwave Workshop Series on RF and Wireless Technologies for Biomedical and Healthcare Applications (IMWS-Bio2014)*, pp. 1–3.
46. **Quresh AM and Mustansar Z** (2017) Levels of detail analysis of microwave scattering from human head models for brain stroke detection. *Peer J* **5**, e4061.
47. **Balanis C** (2005) *Antenna Theory: Analysis and Design*. USA: Wiley-Interscience.
48. **Mobashsher AT and Abbosh AM** (2014) Three-dimensional human head phantom with realistic electrical properties and anatomy. *IEEE Antennas and Wireless Propagation Letters* **13**, 1401–1404.
49. IEEE Recommended Practice for Measurements and Computations of Radio Frequency Electromagnetic Fields With Respect to Human Exposure to Such Fields, 100 kHz–300 GHz. *IEEE Std C95.3-2002 (Revision of IEEE Std C95.3-1991)*, 2002, pp. 1–126.

Payal Bhardwaj received her B.Tech degree in Electronics and Communication Engineering from UP Technical University in the year 2005, and ME degree from Jadvpur University, Kolkata, in Electron Devices in the year 2013. She is pursuing her Ph.D. in the field of Microwave Engineering from Birla Institute of Technology. Currently she is serving as an Assistant Professor in the Electronics and Communication Department of Birla Institute of Technology, Deoghar. Her current research is in the field of design and implementation of printed microstrip antennas for biomedical applications.

Ritesh Kumar Badhai was born in India on 1984. He received the Bachelor of Engineering degree in Electronics and Communication Engineering from Rajiv Gandhi Proudyogiki Vishwavidyalaya, Bhopal, India in 2007. He has completed his Master of Engineering and Ph.D. degree in Electronics and Communication Engineering from Birla Institute of Technology, Mesra, Ranchi, India in 2009 and 2015 respectively. He currently is an Assistant Professor in the Department of Electronics and Communication Engineering, Birla Institute of Technology, Patna, Bihar, India. His research interests are omputational electromagnetics, antenna design, RF circuit design, and EMI/EMC.

https://doi.org/10.1017/S1759078720001579 Published online by Cambridge University Press